SPECIAL EDITION:
RESEARCH ARTICLE:

Africa–UK Partnership for the Computer-aided Development of Sustainable Catalysts
K.T. Malatji, D. Santos-Carballal, U. Terranova, P.E. Ngoepe and N.H. de Leeuw,
S. Afr. J. Chem., 2021, Volume **74** (Special Edition), 3–7,
<https://journals.sabinet.co.za/content/journal/chem/>.

3

Controlling the Lithium Intercalation Voltage in the Li(Mn$_{1-x}$Ni$_x$)$_2$O$_4$ Spinel *via* Tuning of the Ni Concentration: a Density Functional Theory Study

Kemeridge T. Malatji[a] [iD] [§], **David Santos-Carballal**[a,b,c,*] [iD], **Umberto Terranova**[b,d] [iD],
Phuti E. Ngoepe[a] [iD] and **Nora H. de Leeuw**[b,c,e] [iD]

[a]*Materials Modelling Centre, School of Physical and Mineral Sciences, University of Limpopo, Private Bag X1106, Sovenga, 0727, South Africa.*
[b]*School of Chemistry, Cardiff University, Main Building, Park Place, Cardiff CF10 3AT, United Kingdom.*
[c]*School of Chemistry, University of Leeds, Leeds LS2 9JT, United Kingdom.*
[d]*School of Postgraduate Medicine and Allied Health, University of Buckingham, Crewe campus, CW1 5DU, United Kingdom.*
[e]*Department of Earth Sciences, Utrecht University, Princetonplein 8a, 3584 CB Utrecht, Netherlands.*

ABSTRACT

LiMn$_2$O$_4$ spinel is a promising cathode material for secondary lithium-ion batteries. Despite showing a high average voltage of lithium intercalation, the material is structurally unstable, undergoing lowering of the crystal symmetry due to Jahn-Teller distortion of the six-fold Mn^{3+} cations. Although Ni has been proposed as a suitable substitutional dopant to improve the structural stability of LiMn$_2$O$_4$, and enhance the average lithium intercalation voltage, the thermodynamics of the Ni incorporation and its effect on the electrochemical properties of this spinel material are not yet known. In this work, we have employed density functional theory calculations with a Hubbard Hamiltonian (DFT+*U*) to investigate the thermodynamics of cation mixing in the Li(Mn$_{1-x}$Ni$_x$)$_2$O$_4$ solid solution. Our results suggest LiMn$_{1.5}$Ni$_{0.5}$O$_4$ is the most stable composition from room temperature up to at least 1000 K, in agreement with experiments. We also found that the configurational entropy is much lower than the maximum entropy at 1000 K, indicating that higher temperatures are required to reach a fully disordered solid solution. A maximum average lithium intercalation voltage of 4.8 eV was calculated for the LiMn$_{1.5}$Ni$_{0.5}$O$_4$ composition, which is very close to the experimental value. The temperature was found to have a negligible effect on the Li intercalation voltage of the most stable composition. The findings reported here support the application of LiMn$_{1.5}$Ni$_{0.5}$O$_4$ as a suitable cathode material for lithium-ion batteries, with a highly stable voltage of intercalation under a wide range of temperatures.

KEYWORDS

Spinel, equilibrium concentration, mixing thermodynamics, solid-state chemistry and lithium voltage of intercalation.

1. Introduction

The spinel-structured lithium manganese oxide LiMn$_2$O$_4$ (LMO), which can be easily and reversibly de-lithiated, is an environmentally acceptable compound with a low fabrication cost.[1] This material has attracted considerable attention over the last few decades due to its application as a cathode of rechargeable lithium-ion batteries.[2] However, the commercial exploitation of this spinel requires improvement in the relatively low structural stability of its charged form[3] and an increase in the average lithium intercalation voltage. The crystal structure of LMO is severely degraded after a few operational cycles of lithiation and de-lithiation due to the strong Jahn-Teller (JT) distortions of the octahedrally coordinated high-spin Mn^{3+} cations, especially below the Verwey-like temperature (T_V) of 283.5 K.[4] The uneven occupation of the Mn^{3+} e_{g2} state and the interaction with the oxygen p orbitals in LMO causes a tetragonal elongation of this cation in the direction of the d_{z2} orbital which lowers its energy. However, the JT effect vanishes in the de-lithiated MnO$_2$, as all the Mn cations become oxidized to the highly stable 4+ state with a half-filled electronic t_{2g} level.

In the normal LMO spinel, the monovalent Li cations fill the Wyckoff 8*a* tetrahedral holes, while the divalent O atoms form a face-centred cubic (*fcc*) arrangement. Moreover, the Mn ions are embedded in the 16*d* octahedral positions and hold an effective 3.5+ oxidation state. The 3*d* itinerant electrons move freely between the Mn^{3+} and Mn^{4+} cations, which renders these cations equivalent.

Substitutional doping of LMO is an option to avoid the JT-active 3+ oxidation state in the six-fold Mn cations. Replacing the appropriate proportion of this cation by transition metal atoms[5] with a preferred stable oxidation state below 3+ has proven so far to be the best strategy to ensure that manganese is exclusively in the Mn^{4+} form in LMO. For example, 25 %[6] doping by the highly stable Ni^{2+}, with the e_g state half filled, promotes the oxidation of all Mn ions to the JT-inactive 4+ oxidation state. In the discharged spinel, the dopant oxidizes to the very stable low-spin Ni^{4+} with a full t_{2g} level, whereas the rest of the cations remain as Mn^{4+}.

In order to gain detailed atomic-level insight into the doping behaviour of the LMO material, we present here a computational study of the Li(Mn$_{1-x}$Ni$_x$)$_2$O$_4$ solid solution. We have generated the complete configurational space and the inequivalent configurational subspace for each spinel composition and report the mixing thermodynamics and average voltage of lithium intercalation for all the Ni concentrations and its dependence on the temperature for the most energetically stable

* To whom correspondence should be addressed.
E-mail: d.santos-carballal@leeds.ac.uk

SPECIAL EDITION:
RESEARCH ARTICLE:
Africa–UK Partnership for the Computer-aided Development of Sustainable Catalysts
K.T. Malatji, D. Santos-Carballal, U. Terranova, P.E. Ngoepe and N.H. de Leeuw,
S. Afr. J. Chem., 2021, Volume **74** (Special Edition), 3–7,
<https://journals.sabinet.co.za/content/journal/chem/>.

4

composition. We have also determined the cation ordering based on the configurational entropy. The approach presented here shows that moderate Ni doping of the LiMn$_2$O$_4$ leads to a substantial change in the average voltage of lithium intercalation, suggesting an attractive route to tuning the cathode properties of this spinel.

2. Computational Methods

We have carried out spin-polarized density functional theory (DFT) calculations within the Vienna *Ab-initio* Simulation Package (VASP)[7,8] to determine the structures and energies of Li(Mn$_{1-x}$Ni$_x$)$_2$O$_4$. We have employed the Perdew, Burke, and Ernzerhof functional corrected for solids (PBEsol) within the generalized gradient approximation (GGA),[9] where we have included the long-range dispersion corrections *via* the semi-empirical method of Grimme with the Becke and Johnson damping [D3-(BJ)].[10,11] The cut-off for the kinetic energy of the plane wave basis was set at 730 eV , and the effective Hubbard parameters were U_{eff} = 4.0 eV for Mn and 5.5 eV [12] for Ni.[13] A Γ-centred Monkhorst-Pack *k*-point mesh with a uniform spacing of *ca*. 0.16 Å^{-1}, equivalent to a $5 \times 5 \times 5$ grid, was adopted for the Brillouin-zone integrations. To improve the convergence of the electronic partial occupancies during geometry optimizations, we employed the Gaussian and the Methfessel-Paxton order one methods[14] for the spinel phases and lithium metal, respectively, with a smearing width of 0.05 eV . A final static calculation was performed after geometry optimizations using the tetrahedron method with Blöchl corrections to obtain highly accurate energies, as well as the electronic and magnetic properties.[15] The projector augmented wave (PAW) method was used to describe the atomic frozen cores and their interaction with the valence electrons, which were defined as $1s^2 2s^1$ for Li, $3p^6 3d^5 4s^2$ for Mn, $3p^6 3d^8 4s^2$ for Ni and $2s^2 2p^4$ for O. During our simulations, we allowed the relaxation of both the cell shape and internal atomic positions of all structures to their ground state, using the conjugate-gradient method, until the Hellmann–Feynman forces on all atoms dropped below 0.02 eVÅ^{-1}.

The fully lithiated and de-lithiated forms of the nickel-manganese oxide spinel were modelled starting from the conventional cubic unit cell, while the body-centred cubic (*bcc*) lithium was simulated using the asymmetric unit cell. The initial electronic magnetic moments were oriented parallel within the octahedral sub-lattice and were allowed to relax during the simulations. For simplicity, we have used the normal cation arrangement for the spinel phases, where Li occupies the tetrahedral positions, whereas Mn and Ni are confined to the octahedral sites, ignoring the partial inversion degree of x = 0.30 reported experimentally and computationally.[16]

We have used the site occupancy disorder (SOD) code to generate the symmetry-adapted ensemble of configurations within the disordered Li(Mn$_{1-x}$Ni$_x$)$_2$O$_4$ solid solution and to carry out the thermodynamic analysis.[17] Within this approach,

SOD produces the complete configurational space for each Ni concentration in a $1 \times 1 \times 1$ supercell of the conventional cubic unit cell of spinel, followed by a reduction to the sub-space of the symmetrically inequivalent configurations. All configurations were constructed *via* atomic substitutions in LiMn$_2$O$_4$ by using the group of symmetry operators of the space group $Fd\bar{3}m$ (No. 227) of the parent structure. Two configurations are considered equivalent if they can be interconverted following an isometric transformation. Figure 1a represents the extreme LiMn$_2$O$_4$ spinel composition with lattice constant a = 8.34 Å, whereas Fig. 1b shows the extreme LiNi$_2$O$_4$ spinel composition with lattice constant a = 8.03 Å. In the conventional unit cell of the spinel structure, the O atoms are arranged in a face-centred cubic lattice occupying the 32*e* sites, with the tetrahedral (8*a*) cation sites containing Li atoms and the octahedral cation (16*d*) sites filled by the Mn cations. In the configurational space considered for each Ni concentration, the Ni takes up its position in the octahedral 16*d* sites, as shown in Fig. 1c with lattice constant a = 8.22 Å.

3. Results and Discussion

Table 1 displays the prohibitively large total number of configurations (N) for each Ni concentration in the complete configurational space. However, the total number of configurations can be reduced by more than two orders of magnitude to the symmetrically inequivalent configurations (M) in the reduced configurational space. We have chosen to work only with those cell compositions containing an even number of Ni atoms to reduce the number of simulations further.

We have used statistical mechanics to estimate the thermodynamic properties from the sub-space of the symmetrically inequivalent configurations. We have assumed a Boltzmann-like distribution for the estimation of the occurrence probability $\widetilde{P}_m$ at a temperature T of each inequivalent configuration m of energy E_m according to:

$$\widetilde{P}_m = \frac{\Omega_m}{Z}\exp(-E_m/k_B T), \tag{1}$$

Table 1 The total number of configurations (N) and the number of symmetrically inequivalent configurations (M) for each spinel composition in the $1 \times 1 \times 1$ supercell of the cubic unit cell of Li(Mn$_{1-x}$Ni$_x$)$_2$O$_4$.

Cell composition	x	N	M
Li$_8$Mn$_{16}$O$_{32}$	0.0000	1	1
Li$_8$Mn$_{14}$Ni$_2$O$_{32}$	0.1250	120	3
Li$_8$Mn$_{12}$Ni$_4$O$_{32}$	0.2500	1820	22
Li$_8$Mn$_{10}$Ni$_6$O$_{32}$	0.3750	8008	65
Li$_8$Mn$_6$Ni$_{10}$O$_{32}$	0.6250	8008	65
Li$_8$Mn$_4$Ni$_{12}$O$_{32}$	0.7500	1820	22
Li$_8$Mn$_2$Ni$_{14}$O$_{32}$	0.8750	120	3
Li$_8$Ni$_{16}$O$_{32}$	1.0000	1	1
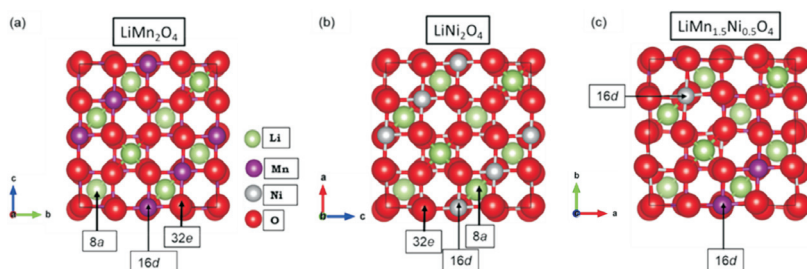
Figure 1 Schematic representation of the conventional unit cells (**a**) LiMn$_2$O$_4$ (**b**) LiNi$_2$O$_4$ and (**c**) LiMn$_{1.5}$Ni$_{0.5}$O$_4$. Lattice geometry and ionic positions for these structures are provided in the Supplementary information.

SPECIAL EDITION:
RESEARCH ARTICLE:

Africa–UK Partnership for the Computer-aided Development of Sustainable Catalysts
K.T. Malatji, D. Santos-Carballal, U. Terranova, P.E. Ngoepe and N.H. de Leeuw,
S. Afr. J. Chem., 2021, Volume **74** (Special Edition), 3–7,
<https://journals.sabinet.co.za/content/journal/chem/>.

5

where Ω_m represents the degeneracy or number of times that a given configuration is repeated in the complete space of all configurations, m can take integer values from 1 to M, k_B is the Boltzmann constant and the configurational partition function $Z = \sum_{m=1}^{M} \Omega_m \exp(-E_m/k_B T)$ ensures that the sum of the probabilities of the complete configurational space is equal to 1.

The Helmholtz free energy of mixing ΔF_{mix} of the solid solution was obtained from:

$$\Delta F_{\text{mix}} = F[\text{Li}(\text{Mn}_{1-x}\text{Ni}_x)_2\text{O}_4 - (1-x)F[\text{LiMn}_2\text{O}_4] - xF[\text{LiNi}_2\text{O}_4] \quad (2)$$

where the configurational free energies $F = -k_B T \ln Z$ were calculated directly from the partition function.

The equilibrium geometries and energies of all configurations in the reduced configurational space of the $\text{Li}(\text{Mn}_{1-x}\text{Ni}_x)_2\text{O}_4$ solid solution were obtained from the DFT calculations. Our results indicate that only one configuration is more stable than the others for the entire Ni concentration range, suggesting a large degree of order within the LiMn_2O_4-LiNi_2O_4 system.

Figure 2 shows the free energy of mixing for the $\text{Li}(\text{Mn}_{1-x}\text{Ni}_x)_2\text{O}_4$ system. Both curves have negative values of ΔF_{mix}, which indicates that the compositions are miscible and can form stable solid solutions. At both 300 K and 1000 K, the same energetically stable structure, at the intermediate Ni composition of $x = 0.25$, has the lowest free energy of mixing. The low free energy of mixing is potentially owing to magnetic interactions, which play a crucial role in the thermodynamics of mixing of these solid solutions, especially at different temperatures. The most stable ordered structure at $x = 0.25$ (–0.93634 eV/cell and –0.92571 eV/cell at 300 and 1000 K, respectively) not only has the lowest energy but it is also weighted most highly, with a probability of occurrence above 99 % at 300 K and 85 % at 1000 K, as compared to the other 21 configurations. Experimentally, $\text{LiMn}_{1.5}\text{Ni}_{0.5}\text{O}_4$ has been suggested as an attractive and promising material because of its acceptable stability, good cyclic property and relatively high capacity.[18] $\text{Li}(\text{Mn}_{1-x}\text{Ni}_x)_2\text{O}_4$ has therefore been the subject of a variety of studies that have reported on synthesis methods, thermal stability, effects of ordered and disordered local structure, cation ordering, particle size, and changes in composition.[19-23]

In Fig. 3, we have plotted the variation of the configurational entropy of the solid solution for $\text{Li}(\text{Mn}_{1-x}\text{Ni}_x)_2\text{O}_4$ with $0 \leq x \leq 1$ as calculated in the $1 \times 1 \times 1$ simulation cell at different temperatures.

The compositions $x = 0$ and $x = 1$ correspond to either Mn or Ni occupancy in all the 16 equivalent octahedral positions in the simulation cell. The configurational entropy is therefore
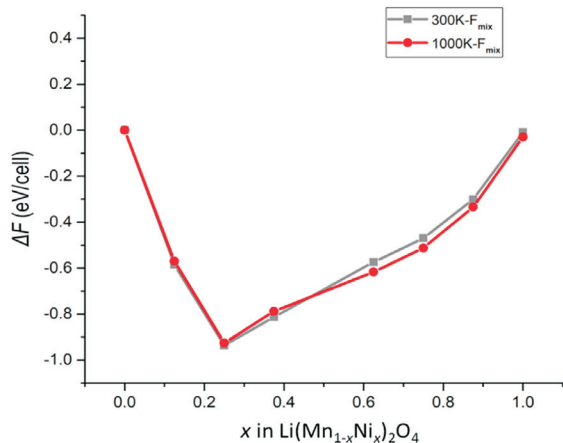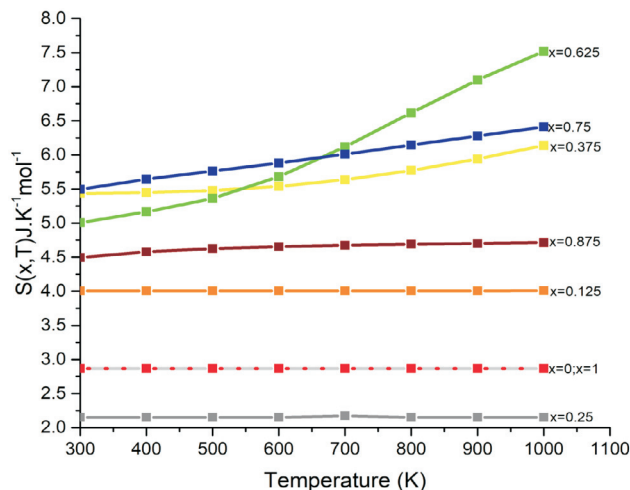

Figure 3 Configurational entropy as a function of temperature for the $1 \times 1 \times 1$ supercell of $\text{Li}(\text{Mn}_{1-x}\text{Ni}_x)_2\text{O}_4$.

independent of the temperature. However, for the remaining concentrations of Ni, and in particular for $x = 0.375$, 0.625 and 0.750, we see that the configurational entropies increase with temperature. At high temperatures, the configurational entropy increasingly tends towards its maximum value, as there are a large number of possible inequivalent configurations for these intermediate Ni concentrations. Interestingly, this configurational entropy behaviour suggests a large degree of site occupancy disorder for the Ni and Mn ions at high temperatures. Experimental investigations of $\text{LiMn}_{1.5}\text{Ni}_{0.5}\text{O}_4$ samples, prepared by annealing at 973.15 K,[24] have shown long-range Ni and Mn ordering, which agrees with our results.

Figure 4 shows schemes of the electronic configuration of the Mn(III, IV) and Ni(II, III, IV) ions when they are located in a high-spin octahedral field of anions. For the pure LiMn_2O_4 spinel, the Mn_B cations have the formal oxidation state 3+ and 4+, represented in Fig. 4a. For the Mn_B cations in both oxidation states, the $t_{2g\uparrow}^3$ level is highly stable since it is half-full.

However, the $t_{2g\uparrow}^1$ orbital has an uneven occupation, which breaks the symmetry of the states and drives the Jahn-Teller distortion of the Mn_B^{3+} ion, which is ultimately responsible for the structural instability of LiMn_2O_4. The Jahn-Teller effect occurs when the non-centrosymmetric lobes of the $d_{x^2-y^2}$ and d_{z^2} orbitals have a different occupation. Note that the empty e_g state of the Mn_B^{4+} cation does not affect the stability of LiMn_2O_4. Figure 4c illustrates the $t_{2g\uparrow}^3 t_{2g\downarrow}^2 e_{2g\uparrow}^2$ and $t_{2g\uparrow}^3 t_{2g\downarrow}^1 e_{2g\uparrow}^2$ electronic distribution of the Ni_B^{3+} and Ni_B^{4+} ions, respectively, in the extreme LiNi_2O_4 composition. As in the lowest energy t_{2g} orbital of the Mn_B(III, IV) ions in LiMn_2O_4, the half-full e_{2g} state of Ni_B(III, IV) is very stable in LiNi_2O_4. Despite the t_{2g} orbitals of Ni_B(III, IV) being partially filled, the reduced stability and symmetry of these ions are not enough to produce a Jahn-Teller distortion. In the case of the d_{xy}, d_{xz} and d_{yz} orbitals with unequal electron populations, their centrosymmetric lobes do not allow Jahn-Teller distortion. For the most stable solid solution with composition $\text{LiMn}_{1.5}\text{Ni}_{0.5}\text{O}_4$, the highly stable electronic distribution of the Mn_B^{4+} ion has already been discussed, which alongside the very stable $t_{2g\uparrow}^3 t_{2g\downarrow}^3 e_{2g\uparrow}^2$ electronic configuration displayed by the Ni_B^{2+} ion, with full t_{2g} and half-full e_{2g} levels, justifies the lowest energy in the free energy of mixing diagram represented in Fig. 2.

Next, we have calculated the average Li intercalation voltage for various Ni concentrations in $\text{Li}(\text{Mn}_{1-x}\text{Ni}_x)_2\text{O}_4$ as:[25,26]

$$\overline{V} = -[E(\text{Li}(\text{Mn}_{1-x}\text{Ni}_x)_2\text{O}_4) - E((\text{Mn}_{1-x}\text{Ni}_x)_2\text{O}_4) - E(\text{Li})] \quad (3)$$

Figure 2 Free energies of mixing (ΔF) for the $\text{Li}(\text{Mn}_{1-x}\text{Ni}_x)_2\text{O}_4$ solid solution at 300 and 1000 K.

SPECIAL EDITION:
RESEARCH ARTICLE:
Africa–UK Partnership for the Computer-aided Development of Sustainable Catalysts
K.T. Malatji, D. Santos-Carballal, U. Terranova, P.E. Ngoepe and N.H. de Leeuw,
S. Afr. J. Chem., 2021, Volume **74** (Special Edition), 3–7,
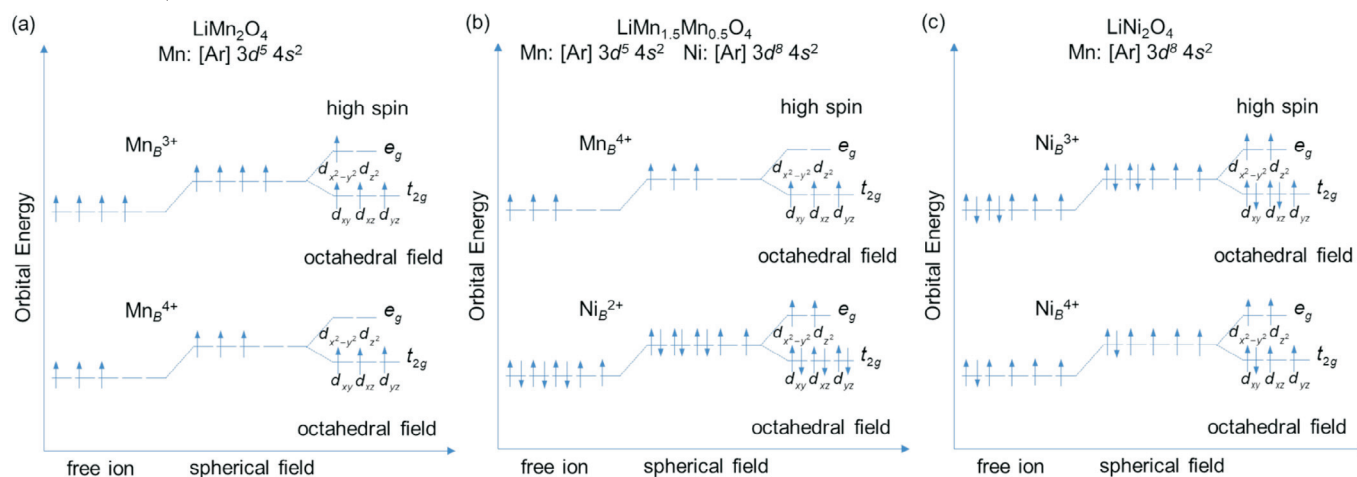<https://journals.sabinet.co.za/content/journal/chem/>.

6

Figure 4 Scheme of the crystal field splitting for the Mn and Ni 3d electrons in high spin octahedral coordination environments (**a**) Mn_B^{3+} and Mn_B^{4+} in $LiMn_2O_4$, (**b**) Mn_B^{4+} and Ni_B^{2+} in $LiMn_{1.5}Ni_{0.5}O_4$ and (**c**) Ni_B^{3+} and Ni_B^{4+} in $LiNi_2O_4$. The perturbation of the Mn and Ni 3d electrons in a spherical field is also represented.

The average voltage of an intercalated compound can be obtained from the Gibbs free energies, which at 0 K can be approximated by the lowest total energies (E) of the lithiated $Li(Mn_{1-x}Ni_x)_2O_4$ structures, compared to the de-lithiated $(Mn_{1-x}Ni_x)_2O_4$ end state and the lowest energy state of pure Li. For the body-centred cubic (*bcc*) Li metal we calculated an optimized lattice constant $a = 3.35$ Å, which is in excellent agreement with experiments.[27,28] Li^+ is preferentially intercalated into tetrahedral sites.

Figure 5 shows the average intercalation voltage for the lowest energy configurations at each Ni concentration, where the voltage changes with the composition of the material. The spinel-structured $LiMn_{1.5}Ni_{0.5}O_4$ (LMNO) has attracted significant attention, owing to its higher working voltage (4.7 V) in comparison with already commercialized cathode materials, such as $LiFePO_4$ (3.4 V), $LiCoO_2$ (3.9 V) and $LiMn_2O_4$ (4.1 V).[29,30] Figure 5 shows how the average voltage of intercalation in $Li(Mn_{1-x}Ni_x)_2O_4$ is related to the energies of the end states (charged and discharged) and varies with Ni concentration. The most energetically stable spinel structure $LiMn_{1.5}Ni_{0.5}O_4$ has a calculated average voltage of 4.866 V, which agrees very well with the experimental operating voltage of ~4.8 V.[1,31] Up to 1000 K, only three configurations have a probability of occurrence that is larger than zero for the most stable Ni composition

($LiMn_{1.5}Ni_{0.5}O_4$), leading to an average Li intercalation voltage that has negligible temperature dependence.

4. Conclusions

We have employed DFT calculations to investigate the effect of substituting nickel for manganese in the $LiMn_2O_4$ cathode material. Our results indicate that any small change in the amount of Ni will be reflected in the stability of the $Li(Mn_{1-x}Ni_x)_2O_4$ spinel. The most stable Ni concentration corresponds to the $LiMn_{1.5}Ni_{0.5}O_4$ stoichiometry, which displays the largest average voltage for the Li intercalation reaction. We found no change in the average voltage for the Li intercalation reaction as the temperature is increased. Our calculations indicate that the lithium intercalation voltage can be modified *via* the control of the Ni concentration in the $Li(Mn_{1-x}Ni_x)_2O_4$ spinel.
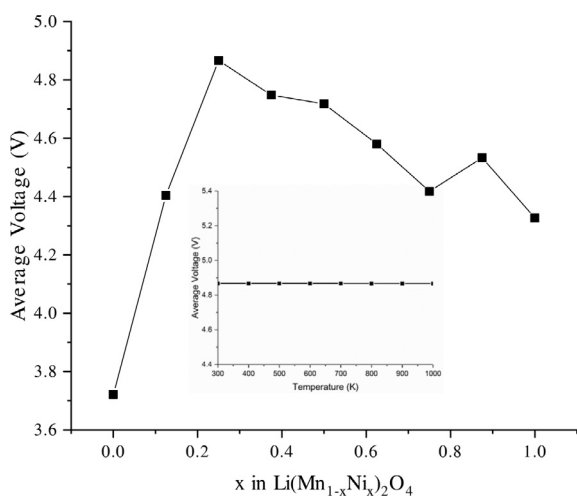
Figure 5 Voltage of Li intercalation for $Li(Mn_{1-x}Ni_x)_2O_4$ as a function of the Ni concentration and (inset) average voltage of lithium intercalation as a function of temperature.

Supplementary Material

Supplementary information is provided in the online supplement.

SPECIAL EDITION:
RESEARCH ARTICLE:
Africa–UK Partnership for the Computer-aided Development of Sustainable Catalysts
K.T. Malatji, D. Santos-Carballal, U. Terranova, P.E. Ngoepe and N.H. de Leeuw,
S. Afr. J. Chem., 2021, Volume **74** (Special Edition), 3–7,
<https://journals.sabinet.co.za/content/journal/chem/>.

7

§ORCID iDs

K.T. Malatji: orcid.org/0000-0001-9071-854X
D. Santos-Carballal: orcid.org/0000-0002-3199-9588
U. Terranova: orcid.org/0000-0001-7380-4737
P.E. Ngoepe: orcid.org/0000-0003-0523-5602
N.H. de Leeuw: orcid.org/0000-0002-8271-0545

References

1 K. Amine, H. Tukamoto, H. Yasuda and Y. Fujita, Preparation and electrochemical investigation of $LiMn_{2-x}Me_xO_4$ (Me: Ni, Fe, and $x=$ 0.5, 1) cathode materials for secondary lithium batteries, *J. Power Sources*, 1997, **68**, 604–608.

2 M.M. Thackeray, W.I.F. David, P.G. Bruce and J.B. Goodenough, Lithium insertion into manganese spinels, *Mater. Res. Bull.*, 1983, **18**, 461–472.

3 E. Iwata, K. Takahashi, K. Maeda and T. Mouri, Capacity failure on cycling or storage of lithium-ion batteries with Li–Mn–O ternary phases having spinel-framework structure and its possible solution, *J. Power Sources*, 1999, **81–82**, 430–433.

4 I. Tomeno, Y. Kasuya and Y. Tsunoda, Charge and spin ordering in $LiMn_2O_4$, *Phys. Rev. B*, 2001, **64**, 094422.

5 F.X. Wang, S.Y. Xiao, Y. Shi, L.L. Liu, Y.S. Zhu, Y.P. Wu, J.Z. Wang and R. Holze, Spinel $LiNi_xMn_{2-x}O_4$ as cathode material for aqueous rechargeable lithium batteries, *Electrochim. Acta*, 2013, **93**, 301–306.

6 M. Michalska, D.A. Ziołkowska, J.B. Jasinski, P.-H. Lee, P. Ławniczak, B. Andrzejewski, A. Ostrowski, W. Bednarski, S.-H. Wu and J.-Y. Lin, Improved electrochemical performance of $LiMn_2O_4$ cathode material by Ce doping, *Electrochim. Acta*, 2018, **276**, 37–46.

7 G. Kresse and J. Furthmüller, Efficient iterative schemes for ab initio total-energy calculations using a plane-wave basis set, *Phys. Rev. B*, 1996, **16**, 11169–11186.

8 G. Kresse and J. Furthmüller, Efficiency of ab-initio total energy calculations for metals and semiconductors using a plane-wave basis set, *Comput. Mater. Sci.*, 1996, **6**, 15–50.

9 J.P. Perdew, A. Ruzsinszky, G.I. Csonka, O.A. Vydrov, G.E. Scuseria, L.A. Constantin, X. Zhou and K. Burke, Restoring the density-gradient expansion for exchange in solids and surfaces, *Phys. Rev. Lett.*, 2008, **100**, 136406.

10 S. Grimme, S. Ehrlich and L. Goerigk, Effect of the damping function in dispersion corrected density functional theory, *J. Comput. Chem*, 2011, **32**, 1456–1465.

11 S. Grimme, J. Antony, S. Ehrlich and H. Krieg, A consistent and accurate ab initio parametrisation of density functional dispersion correction (DFT-D) for the 94 elements H-Pu, *J. Chem. Phys.*, 2010, **132**, 154104.

12 D. Santos-Carballal, A. Roldan, R. Grau-Crespo and N.H. de Leeuw, First-principles study of the inversion thermodynamics and electronic structure of FeM_2X_4 (thio)spinels (M = Cr, Mn, Co, Ni; X = O, S), *Phys. Rev. B*, 2015, **91**, 195106.

13 S.L. Dudarev, G.A. Botton, S.Y. Savrasov, C.J. Humphreys and A.P. Sutton, Electron-energy-loss spectra and the structural stability of nickel oxide: an LSDA+U study., *Phys. Rev. B*, 1998, **57**, 1505 –1509.

14 M. Methfessel and A.T. Paxton, High-precision sampling for Brillouin-zone integration in metals, *Phys. Rev. B*, 1989, **40**, 3616–3621.

15 P.E. Blochl, O. Jepsen and O.K. Andersen, Improved tetrahedron method for Brillouin-zone integrations, *Phys. Rev.*, 1994, **49**, 16223–16233.

16 D. Santos-Carballal, P.E. Ngoepe and N.H. de Leeuw, *Ab initio* investigation of the thermodynamics of cation distribution and of the electronic and magnetic structures in the $LiMn_2O_4$ spinel, *Phys. Rev. B*, 2018, **97**, 085126.

17 R. Grau-Crespo, S. Hamad, C.R.A. Catlow and N.H. de Leeuw, Symmetry-adapted configurational modelling of fractional site occupancy in solids, *J. Phys.: Condens. Matter*, 2007, **19**, 256201.

18 H. Wang, H. Xia, M.O. Lai and L. Lu, Enhancements of rate capability and cyclic performance of spinel $LiNi_{0.5}Mn_{1.5}O_4$ by trace Ru-doping, *Electrochem. Commun.*, 2009, **11**, 1539–1542.

19 M. Kunduraci and G.G. Amatucci, Effect of oxygen nonstoichiometry and temperature on cation ordering in $LiMn_{2-x}Ni_xO_4$ (0.50 = x = 0.36) spinels, *J. Power Sources*, 2007, **165**, 359–367.

20 A. Sakunthala, M.V Reddy, S. Selvasekarapandian, B.V.R. Chowdari and P. Christopher, Synthesis of compounds, $Li(MMn_{11/6})O_4$ (M = $Mn_{1/6}$, $Co_{1/6}$, $(Co_{1/12}Cr_{1/12})$, $(Co_{1/12}Al_{1/12})$, $(Cr_{1/12}Al_{1/12})$) by polymer precursor method and its electrochemical performance for lithium-ion batteries, *Electrochim. Acta*, 2010, **55**, 4441–4450.

21 E. Hu, S.M. Bak, J. Liu, X. Yu, Y. Zhou, S.N. Ehrlich, X.Q. Yang and K.W. Nam, Oxygen-release-related thermal stability and decomposition pathways of $Li_xNi_{0.5}Mn_{1.5}O_4$ cathode materials, *Chem. Mater.*, 2014, **26**, 1108–1118.

22 G.B. Zhong, Y.Y. Wang, X.J. Zhao, Q.S Wang, Y. Yu and C.H. Chen, Structural, electrochemical and thermal stability investigations on $LiNi_{0.5-x}Al_{2x}Mn_{1.5-x}O_4$ (0 ≤ 2x ≤ 1.0) as 5 V cathode materials, *J. Power Sources*, 2012, **216**, 368–375.

23 J. Bréger, K. Kang, J. Cabana, G. Ceder and C.P. Grey, NMR, PDF and RMC study of the positive electrode material $Li(Ni_{0.5}Mn_{0.5})O_2$ synthesised by ion-exchange methods, *J. Mater. Chem.*, 2007, **17**, 3167–3174.

24 J. Song, D.W. Shin, Y. Lu, C.D. Amos, A. Manthiram and J.B. Goodenough, Role of oxygen vacancies on the performance of $Li[Ni_{0.5-x}Mn_{1.5+x}]O_4$ (x = 0, 0.05, and 0.08) spinel cathodes for lithium-ion batteries, *Chem. Mater.*, 2012, **24**, 3101–3109.

25 J. Bhattacharya and C. Wolverton, Relative Stability of normal vs. inverse spinel for 3d transition metal oxides as lithium intercalation cathodes, *Phys. Chem. Chem. Phys.*, 2013, **15**, 6486–6498.

26 M.K. Aydinol and G. Ceder, First-principles prediction of insertion potentials in Li-Mn oxides for secondary Li batteries, *Electrochem. Soc.*, 1997, **144**, 3832–3835.

27 C.S. Barrett, A low temperature transformation in lithium. *Phys. Rev.*, 1947, **72**, 245.

28 C.S. Barrett, X-ray study of alkaline metal at low temperatures, *Acta Crystallogr.*, 1956, **9**, 671–677.

29 S. Hy, H. Liu, M. Zhang, D. Qian, B.-J. Hwang and Y.S. Meng, Performance and design considerations for lithium excess layered oxide positive electrode materials for lithium-ion batteries, *Energy Environ. Sci.*, 2016, **9**, 1931–1954.

30 A. Kraytsberg and Y. Ein-Eli, Higher, stronger, better… A review of 5 volt cathode materials for advanced lithium-ion batteries, *Adv. Energy Mater.*, 2012, **2**, 922–939.

31 Q. Zhong, A. Bonakdarpour, M. Zhang, Y. Gao and J.R. Dahn, Synthesis and electrochemistry of $LiNi_xMn_{2-x}O_4$, *J. Electrochem. Soc.*, 1997, **205**, 205–213.

Supplementary information, *S. Afr. J. Chem.*

Controlling the lithium intercalation voltage in the Li(Mn$_{1-x}$Ni$_x$)$_2$O$_4$ spinel via tuning of the Ni concentration: a Density Functional Theory study

Kemeridge T. Malatji[a], David Santos-Carballal[a,b,c,*], Umberto Terranova[b,d], Phuti E. Ngoepe[a], and Nora H. de Leeuw[b,c,e,†]

[a]*Materials Modelling Centre, School of Physical and Mineral Sciences, University of Limpopo, Private Bag x 1106, Sovenga, 0727, South Africa*

[b]*School of Chemistry, Cardiff University, Main Building, Park Place, Cardiff CF10 3AT, UK*

[c]Present address: School of Chemistry, University of Leeds, Leeds LS2 9JT, United Kingdom

[d]*School of Postgraduate Medicine and Allied Health, University of Buckingham, Crewe campus, CW1 5DU, United Kingdom*

[e]*Department of Earth Sciences, Utrecht University, Princetonplein 8a, 3584 CB Utrecht, The Netherlands*

TABLE OF CONTENTS

* D.Santos-Carballal@leeds.ac.uk

† deLeeuwN@cardiff.ac.uk; N.H.deLeeuw@leeds.ac.uk; N.H.deLeeuw@uu.nl

1. Optimised lattice geometry and ionic positions for LiMn$_2$O$_4$

Format: VASP POSCAR file

```
Li Mn O
   1.0000000000000000
     8.3395017889305052     0.0000000000000000    -0.0000000000000000
     0.0000000000000000     8.3395017889305052    -0.0000000000000000
    -0.0000000000000000     0.0000000000000000     8.3395017889305052
    Li   Mn    O
     8    16    32
Direct
  0.1250000000000000   0.1250000000000000   0.1250000000000000
  0.6250000000000000   0.1250000000000000   0.6250000000000000
  0.1250000000000000   0.6250000000000000   0.6250000000000000
  0.6250000000000000   0.6250000000000000   0.1250000000000000
  0.8750000000000000   0.3750000000000000   0.3750000000000000
  0.8750000000000000   0.8750000000000000   0.8750000000000000
  0.3750000000000000   0.3750000000000000   0.8750000000000000
  0.3750000000000000   0.8750000000000000   0.3750000000000000
  0.5000000000000000   0.5000000000000000   0.5000000000000000
  0.2500000000000000   0.7500000000000000   0.0000000000000000
  0.7500000000000000   0.0000000000000000   0.2500000000000000
  0.0000000000000000   0.2500000000000000   0.7500000000000000
  0.7500000000000000   0.2500000000000000   0.0000000000000000
  0.2500000000000000   0.0000000000000000   0.7500000000000000
  0.0000000000000000   0.7500000000000000   0.2500000000000000
  0.5000000000000000   0.0000000000000000   0.0000000000000000
  0.2500000000000000   0.2500000000000000   0.5000000000000000
  0.7500000000000000   0.5000000000000000   0.7500000000000000
  0.7500000000000000   0.7500000000000000   0.5000000000000000
  0.2500000000000000   0.5000000000000000   0.2500000000000000
  0.0000000000000000   0.5000000000000000   0.0000000000000000
  0.5000000000000000   0.2500000000000000   0.2500000000000000
  0.5000000000000000   0.7500000000000000   0.7500000000000000
  0.0000000000000000   0.0000000000000000   0.5000000000000000
  0.2621894965390581   0.2621894965390581   0.2621894965390581
  0.4878105034609419   0.9878105034609419   0.7621894965390581
  0.9878105034609419   0.7621894965390581   0.4878105034609419
  0.7621894965390581   0.4878105034609419   0.9878105034609419
  0.0121894965390581   0.5121894965390581   0.2378105034609419
  0.7378105034609419   0.7378105034609419   0.7378105034609419
  0.5121894965390581   0.2378105034609419   0.0121894965390581
  0.2378105034609419   0.0121894965390581   0.5121894965390581
  0.5121894965390581   0.0121894965390581   0.2378105034609419
  0.0121894965390581   0.2378105034609419   0.5121894965390581
  0.2378105034609419   0.5121894965390581   0.0121894965390581
  0.9878105034609419   0.4878105034609419   0.7621894965390581
  0.4878105034609419   0.7621894965390581   0.9878105034609419
  0.7621894965390581   0.9878105034609419   0.4878105034609419
  0.2621894965390581   0.7621894965390581   0.7621894965390581
  0.4878105034609419   0.4878105034609419   0.2621894965390581
  0.9878105034609419   0.2621894965390581   0.9878105034609419
  0.0121894965390581   0.0121894965390581   0.7378105034609419
  0.7378105034609419   0.2378105034609419   0.2378105034609419
  0.5121894965390581   0.7378105034609419   0.5121894965390581
  0.5121894965390581   0.5121894965390581   0.7378105034609419
  0.0121894965390581   0.7378105034609419   0.0121894965390581
  0.9878105034609419   0.9878105034609419   0.2621894965390581
  0.4878105034609419   0.2621894965390581   0.4878105034609419
  0.7621894965390581   0.2621894965390581   0.7621894965390581
  0.2621894965390581   0.4878105034609419   0.4878105034609419
  0.2378105034609419   0.7378105034609419   0.2378105034609419
```

2. Optimised lattice geometry and ionic positions for LiNi$_2$O$_4$

Format: VASP POSCAR file


```
Li Ni O
   1.0000000000000000
     8.0317498321027472     0.0000000000000000     0.0000000000000000
    -0.0000000000000000     8.0317498321027472     0.0000000000000000
    -0.0000000000000000    -0.0000000000000000     8.0317498321027472
    Li   Ni    O
     8    16    32
Direct
  0.1250000000000000  0.1250000000000000  0.1250000000000000
  0.6250000000000000  0.1250000000000000  0.6250000000000000
  0.1250000000000000  0.6250000000000000  0.6250000000000000
  0.6250000000000000  0.6250000000000000  0.1250000000000000
  0.8750000000000000  0.3750000000000000  0.3750000000000000
  0.8750000000000000  0.8750000000000000  0.8750000000000000
  0.3750000000000000  0.3750000000000000  0.8750000000000000
  0.3750000000000000  0.8750000000000000  0.3750000000000000
  0.5000000000000000  0.5000000000000000  0.5000000000000000
  0.2500000000000000  0.7500000000000000  0.0000000000000000
  0.7500000000000000  0.0000000000000000  0.2500000000000000
  0.0000000000000000  0.2500000000000000  0.7500000000000000
  0.7500000000000000  0.2500000000000000  0.0000000000000000
  0.2500000000000000  0.0000000000000000  0.7500000000000000
  0.0000000000000000  0.7500000000000000  0.2500000000000000
  0.5000000000000000  0.0000000000000000  0.0000000000000000
  0.2500000000000000  0.2500000000000000  0.5000000000000000
  0.7500000000000000  0.5000000000000000  0.7500000000000000
  0.7500000000000000  0.7500000000000000  0.5000000000000000
  0.2500000000000000  0.5000000000000000  0.2500000000000000
  0.0000000000000000  0.5000000000000000  0.0000000000000000
  0.5000000000000000  0.2500000000000000  0.2500000000000000
  0.5000000000000000  0.7500000000000000  0.7500000000000000
  0.0000000000000000  0.0000000000000000  0.5000000000000000
  0.2627472841061365  0.2627472841061365  0.2627472841061365
  0.4872527158938635  0.9872527158938634  0.7627472841061366
  0.9872527158938634  0.7627472841061366  0.4872527158938635
  0.7627472841061366  0.4872527158938635  0.9872527158938634
  0.0127472841061365  0.5127472841061366  0.2372527158938635
  0.7372527158938634  0.7372527158938634  0.7372527158938634
  0.5127472841061366  0.2372527158938635  0.0127472841061365
  0.2372527158938635  0.0127472841061365  0.5127472841061366
  0.5127472841061366  0.0127472841061365  0.2372527158938635
  0.0127472841061365  0.2372527158938635  0.5127472841061366
  0.2372527158938635  0.5127472841061366  0.0127472841061365
  0.9872527158938634  0.4872527158938635  0.7627472841061366
  0.4872527158938635  0.7627472841061366  0.9872527158938634
  0.7627472841061366  0.9872527158938634  0.4872527158938635
  0.2627472841061365  0.7627472841061366  0.7627472841061366
  0.4872527158938635  0.4872527158938635  0.2627472841061365
  0.9872527158938634  0.2627472841061365  0.9872527158938634
  0.0127472841061365  0.0127472841061365  0.7372527158938634
  0.7372527158938634  0.2372527158938635  0.2372527158938635
  0.5127472841061366  0.7372527158938634  0.5127472841061366
  0.5127472841061366  0.5127472841061366  0.7372527158938634
  0.0127472841061365  0.7372527158938634  0.0127472841061365
  0.9872527158938634  0.9872527158938634  0.2627472841061365
  0.4872527158938635  0.2627472841061365  0.4872527158938635
  0.7627472841061366  0.2627472841061365  0.7627472841061366
  0.2627472841061365  0.4872527158938635  0.4872527158938635
  0.2372527158938635  0.7372527158938634  0.2372527158938635
```

3. Optimised lattice geometry and ionic positions for LiMn$_{1.5}$Ni$_{0.5}$O$_4$

Format: VASP POSCAR file

```
Li Ni Mn O
   1.0000000000000000
     8.2061908316793666     0.0259489110133812     0.0000000000000000
     0.0259489110133812     8.2061908316793666     0.0000000000000000
    -0.0000000000000000    -0.0000000000000000     8.4146280562520612
    Li   Ni   Mn   O
     8    4    12    32
Direct
  0.1208566457535635   0.1214847681639917   0.1207376360905351
  0.6291433542464364   0.1285152318360083   0.6207376360905351
  0.1287343998670981   0.6245290363758530   0.6212999452454613
  0.6212656001329019   0.6254709636241470   0.1212999452454613
  0.8714847681639917   0.3708566457535635   0.3792623639094578
  0.8785152318360083   0.8791433542464364   0.8792623639094649
  0.3745290363758530   0.3787343998670981   0.8787000547545387
  0.3754709636241470   0.8712656001329019   0.3787000547545387
  0.5009602047960844   0.4990397952039228   0.5000000000000000
  0.2490397952039157   0.7509602047960844   0.0000000000000000
  0.7469006805754552   0.9969006805754552   0.2500000000000000
  0.0030993194245448   0.2530993194245448   0.7500000000000000
  0.7471693900688734   0.2528306099311267   0.0000000000000000
  0.2528200239625895   0.0025174945206890   0.7516578649458704
  0.9974825054793111   0.7471799760374105   0.2483421350541297
  0.5004609503732514   0.0025482092504695   0.9947603169566815
  0.2495390496267486   0.2474517907495305   0.4947603169566815
  0.7525174945206889   0.5028200239625895   0.7483421350541296
  0.7525482092504695   0.7504609503732514   0.5052396830433185
  0.2466956790159850   0.4966956790159850   0.2500000000000000
  0.9974517907495305   0.4995390496267486   0.0052396830433185
  0.4971799760374105   0.2474825054793110   0.2516578649458703
  0.5033043209840150   0.7533043209840150   0.7500000000000000
  0.0028306099311266   0.9971693900688734   0.5000000000000000
  0.2594366584243758   0.2578711892518081   0.2632387860462411
  0.4905633415756242   0.9921288107481918   0.7632387860462411
  0.9893271365721110   0.7569311547991920   0.4821093364024664
  0.7606728634278890   0.4930688452008080   0.9821093364024663
  0.0078711892518081   0.5094366584243758   0.2367612139537589
  0.7421288107481918   0.7405633415756242   0.7367612139537589
  0.5069311547991920   0.2393271365721110   0.0178906635975336
  0.2430688452008079   0.0106728634278961   0.5178906635975337
  0.5055918570291146   0.0090507566140311   0.2274533675383855
  0.0191372323491933   0.2328835331710633   0.4951661426746514
  0.2299453295942063   0.5003605027529520   0.0212307912301326
  0.9909492433859689   0.4944081429708854   0.7725466324616145
  0.4996394972470480   0.7700546704057937   0.9787692087698674
  0.7671164668289367   0.9808627676508067   0.5048338573253486
  0.2703903077351128   0.7685280740030340   0.7524991481922543
  0.4796096922648872   0.4814719259969660   0.2524991481922543
  0.9828835331710633   0.2691372323491933   0.0048338573253486
  0.0236448852389072   0.0154758265708955   0.7555768004382646
  0.7263551147610928   0.2345241734291045   0.2555768004382646
  0.5200546704057937   0.7496394972470480   0.5212307912301326
  0.5185280740030340   0.5203903077351127   0.7475008518077457
  0.9987147862501721   0.7326411559537384   0.0216673639060260
  0.9845241734291045   0.9763551147610928   0.2444231995617354
  0.4826411559537384   0.2487147862501720   0.4783326360939740
  0.7654758265708955   0.2736448852389072   0.7444231995617354
  0.2503605027529520   0.4799453295942134   0.4787692087698674
  0.2314719259969660   0.7296096922648873   0.2475008518077457
```

4